Multi-phase simulation of infected respiratory cloud transmission in air

Diana De Padova, and Michele Mossa

View Online   Export Citation   CrossMark

open access

AIP Advances Photonics and Optics Collection   READ NOW!

AIP Publishing

Multi-phase simulation of infected respiratory cloud transmission in air

View Online   Export Citation   CrossMark

Diana De Padova[a] (iD) and Michele Mossa (iD)

AFFILIATIONS

DICATECh - Department of Civil, Environmental, Land, Building Engineering and Chemistry, Polytechnic University of Bari,
Via E. Orabona 4, 70125 Bari, Italy

[a]Author to whom correspondence should be addressed: diana.depadova@poliba.it

ABSTRACT

In the face of the increasing death toll of the COVID-19 global pandemic, countries around the world have instituted restrictive measures to mitigate the serious effects of the pandemic. Human-to-human transmission of COVID-19 occurs primarily through large droplets that are expelled with sufficient momentum to come in direct contact with the recipients' mouth. Therefore, the physics of flow is central to transmission of COVID-19. Respiratory infections increase the frequency of violent expiration, including coughing and sneezing that are particularly effective in dispersing virus-carrying droplets. Moreover, the high viral load in droplets of asymptomatic hosts that are expelled during respiratory activities is contributing to the rapid growth of the COVID-19 global pandemic. The present study uses 2D smoothed-particle-hydrodynamics multi-phase simulations of the fluid dynamics of violent expiratory events in order to obtain a deeper understanding of the multi-phase nature of respiratory clouds, which can help determine separation distances from an infected person needed to minimize respiratory transmission. Our results indicate that there are three phases of jet cloud flow: the first is dominated by no-buoyancy jet-like dynamics characterized by a high speed, the second is dominated by negative buoyancy, and the third is dominated by gravity that deflects the cloud downward. Moreover, two modes of jet behavior that differ in dilution have been identified to be a function of distance from the human mouth. This work is of direct relevance to studies on the spread of COVID-19 and similar outbreaks in the future.

I. INTRODUCTION

Today, unfortunately, COVID-19 is affecting territories around the world, causing a global economic crisis. The COVID-19 pandemic is, first and foremost, a health crisis. Worldwide, there have been about 2.06×10^6 deaths. However, it has rapidly become an economic crisis too. Over the past year, there has been a continuous reduction in the activities and movements of a vast majority of people. All politicians are today on the frontline of this fight against a virus that knows no borders.

Today, even breathing fresh air in a park, at the countryside, or in the mountains (where social distancing can easily be observed) seems to carry the risk of contagion. During human expiratory activities such as talking, laughing, coughing, and sneezing, many droplets of saliva and other secretions are expelled from the respiratory tract via the mouth and nose. Many studies[1–6] have shown how movement of droplets during human respiratory activities plays a key role in the transmission of respiratory infectious diseases.

Likewise, the virus responsible for COVID-19, SARS-CoV-2, is transmitted through natural respiratory activities such as breathing, talking, laughing, coughing, and sneezing.[7–9] Therefore, an understanding of the fluid dynamics of expiratory virus-laden droplets is needed to accurately predict virus transmission. Recent work has demonstrated that exhalation, sneezing, and coughing not only produce mucosalivary droplets that follow short-range semi-ballistic trajectories but, importantly, also produce a multi-phase turbulent gas cloud (a puff) that consists of ambient air that traps and carries clusters of droplets that have a continuum of sizes within it. In fact, the transmission process is characterized by complex flow phenomena ranging from air–mucous interactions, turbulent jets, and droplet evaporation and deposition to flow-induced particle dispersion and sedimentation.[7]

Flow physics is central to the transmission of COVID-19, and much of the recent work in this area has exploited the power of computational fluid dynamics modeling. Multi-phase flows give rise to a

rich variety of physical phenomena, with applications in many fields of engineering, for example, aerodynamics,[10] biomedical flows,[11–14] and bed load transport and sedimentation.[15–17]

During the last year, multi-phase flows of violent expiratory events have been investigated using fully coupled Eulerian–Lagrangian techniques. In the study by Pendar and Páscoa,[4] a comprehensive fully coupled Eulerian–Lagrangian method has been applied, showing that the movement of the expelled droplets is mainly influenced by their size, angle, velocity, and environmental factors. Dbouk and Drikakis[18] employed an advanced three-dimensional model based on fully coupled Eulerian–Lagrangian techniques that take into account the influence of environmental parameters on the infected respiratory cloud transmission in air.

However, to overcome the limitations typical of grid-based models,[19] an alternative numerical approach for multi-phase flows can be based on meshless methods such as Smoothed Particle Hydrodynamics (SPH). Meshless Lagrangian techniques appear, in general, to be more suitable in capturing the highly unsteady free surface. With the Lagrangian description, the convective terms are incorporated into the velocity derivative (with respect to time), and the distribution of the points used for discretization evolves according to the governing equations. This feature allows for the modeling of discontinuous fluid domains, free-surface flows, and multi-phase flows. In the SPH technique, materials with different physical properties can easily coexist within the same domain. They are discretized by convenient particle sets, each characterized by specific physical properties and constitutive laws. Each interface between different materials is automatically considered by extending the summation to all particles located at a distance shorter than 2h (with h being the smoothing length) from the point where the flow variables and their derivatives are required. A number of insights obtained from Smoothed Particle Hydrodynamics (SPH) have shown that this method can be successfully applied to the simulation of several fluid-dynamics problems with highly nonlinear deformations, such as the breaking and impact of waves,[20–23] hydraulic jumps,[24–27]

multi-phase flows,[28,29] spilling breakers and bore propagation,[30,31] fluid–structure interaction (FSI) problems,[19,32] and oscillating jets that induce breaking waves.[33–35] In this study, the SPH approach was employed to study coughing and sneezing processes with the aim of evaluating the effectiveness of social limitations used to optimize the safety of individuals. This paper contributes to understanding the dilution curve of a sneeze event, which is one of the major sources of pathogen-carrying droplets in indoor air.

II. SPH NUMERICAL METHOD

As a Lagrangian method, SPH simulates the domain as a set of discrete particles. To find the value of $\boldsymbol{a}(\bar{\boldsymbol{x}}, t)$ at a generic point $\bar{\boldsymbol{x}}$, an interpolation is applied from the nodal values $a_i(t)$ through a kernel function $\boldsymbol{W} = (\boldsymbol{x} - \bar{\boldsymbol{x}}, \eta)$ as follows:

$$\boldsymbol{a}(\bar{\boldsymbol{x}}, t) \approx \langle \boldsymbol{a}(\bar{\boldsymbol{x}}, t)\rangle = \sum_{j=1}^{N} \frac{m_j}{\rho_j} \boldsymbol{a}(\boldsymbol{x}_j, t) W(\boldsymbol{x}_j - \bar{\boldsymbol{x}}, \eta), \qquad (1)$$

where ρ is the fluid density and the summation is extended to all N particles located inside the sphere of radius 2η centered on $\bar{\boldsymbol{x}}$.

The advantage of the SPH approach is that a differential operator applied to $\boldsymbol{a}(\bar{\boldsymbol{x}}, t)$ can be approximated by making use of the gradient of the kernel function as follows:

$$\nabla \cdot \boldsymbol{a}(\bar{\boldsymbol{x}}, t) \approx \langle \nabla \cdot \boldsymbol{a}(\bar{\boldsymbol{x}}, t)\rangle = \sum_{j=1}^{N} \frac{m_j}{\rho_j} [\boldsymbol{a}(\bar{\boldsymbol{x}}, t) - \boldsymbol{a}(\boldsymbol{x}_j, t)] \nabla W(\boldsymbol{x}_j - \bar{\boldsymbol{x}}, \eta). \qquad (2)$$

Including multiple phases in SPH is relatively straightforward as it is possible to assign a separate set of particles to each phase with minimal treatment of the interface.

The multi-phase flow is described by the Reynolds-averaged Navier–Stokes (RANS) equations. Using the modified version of Tait's equation of state for the air phase,[36] the governing equations in the Lagrangian frame take the following form:

$$
\begin{cases}
\left\langle \dfrac{D\rho_i}{Dt}\right\rangle = \sum_j m_j(\boldsymbol{v}_i - \boldsymbol{v}_j)\cdot \hat{\nabla} W_{ij}, & \\[2mm]
\left\langle \dfrac{D\boldsymbol{v_i}}{Dt}\right\rangle = -\sum_j m_j\left(\dfrac{p_i}{\rho_i^2} + \dfrac{p_j}{\rho_j^2}\right)\nabla W_{ij} + \sum_j m_j(\mathcal{T}_i - \mathcal{T}_j)\cdot\hat{\nabla} W_{ij} + \boldsymbol{g} & (water\ phase), \\[2mm]
\left\langle \dfrac{D\boldsymbol{v_i}}{Dt}\right\rangle = -\sum_j m_j\left(\dfrac{p_i}{\rho_i^2} + \dfrac{p_j}{\rho_j^2}\right)\nabla W_{ij} - 2a\rho_a^2\dfrac{m_i}{\rho_i^2}\nabla W_{ij} + \sum_j m_j(\mathcal{T}_i - \mathcal{T}_j)\cdot\hat{\nabla} W_{ij} + \boldsymbol{g} & (air\ phase), \\[2mm]
\mathcal{T}_i = \mu_{T_i}\mathcal{S}_i, &
\end{cases}
\qquad (3)
$$

where ρ is the density, $\boldsymbol{v}$ is the velocity vector, p is the pressure, g is the gravity acceleration vector, ρ_a is the initial density of the air phase, $\mathcal{T}$ is the turbulent shear stress tensor, $\mathcal{S}$ is the rate-of-strain tensor, and μ_T is the dynamic eddy viscosity.

The turbulent stresses are represented by a two-equation k–ε model.[37] The SPH k–ε model was described in the study by De Padova *et al.*[25] to which the reader is referred to for further details. The semi-discrete system [Eq. (3)] is integrated in time by a

second-order two-stage XSPH explicit algorithm[38] where each particle is moved according to a velocity

$$\boldsymbol{v}_i^X = \varphi \sum_j \frac{m_j}{\rho_j}\boldsymbol{v}_j\hat{W}_{ij} + (1 - \varphi)\boldsymbol{v}_i^{n+1}, \qquad (4)$$

where φ is a velocity smoothing coefficient and $\boldsymbol{v}_i^{n+1}$ is the value obtained by solving the second and third equations of Eq. (3). The
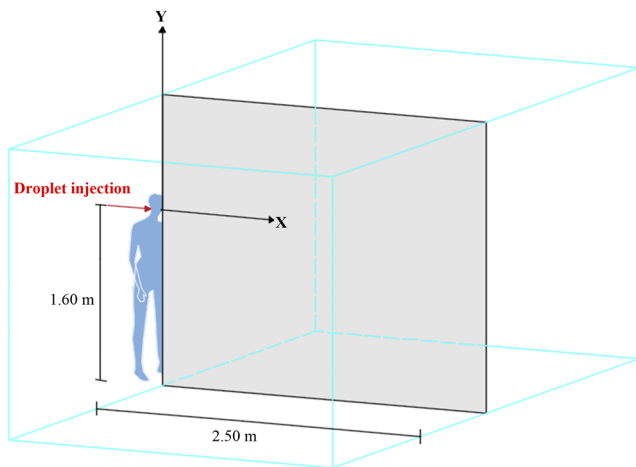
FIG. 1. Computational domain.

time step varies slightly during the simulation in order to guarantee the following Courant stability condition: $CFL = \Delta t \frac{\max_i (v_i + c_i)}{h} \leq 0.2$. Further details about the SPH technique can be found in the study by Gomez-Gesteira.[39]

III. NUMERICAL TESTS

In this study, only coughing and sneezing are considered as they are the major sources of pathogen-carrying droplets in indoor

air.[40–47] In order to capture the dynamic characteristics of the dispersion of droplets by coughing and sneezing, 2D SPH simulations were carried out using a validated Weakly Compressible SPH (WCSPH) scheme.

The transport characteristics of droplets produced by coughing and sneezing are examined in tests T1 and T2, respectively. A 2D computational domain representing a rectangular space in front of a coughing/sneezing person was assumed, as shown in Fig. 1. The computational domain was large enough to represent a real room. The domain was then discretized using an initial particle spacing equal to 0.005 m with 140 000 particles. Droplets were injected through a nozzle located 1.6 m above the floor (Fig. 1). In the simulations, no distinction is made between physical and aerodynamic diameters, and therefore, the particle jet is modeled as a continuum flow.

The initial velocity, human mouth opening, volume, and other parameters recorded for clinical coughs and sneezes have been taken from the literature (see Tables I and II). No ventilation was included in either test (T1 or T2) in order to create a quasi-quiescent environment, and the droplet and air temperatures were assumed to be 32 °C and 20 °C, respectively.[48,49] The nozzle diameter d was 2 cm, representing the diameter of a human mouth during coughing/sneezing.[44–48]

Recent studies demonstrated that exhalations, sneezes, and coughs not only consist of mucosalivary droplets that follow short-range semi-ballistic trajectories but, importantly, also are primarily made up of a multi-phase turbulent gas cloud (a puff) that consists of ambient air that traps and carries clusters of droplets with

TABLE I. Principal parameters of test T1.

T1—cough		
Temperature (T)	32 °C with 20° ambient	Zhu et al.[48,49]
Average expiration air velocity during coughing U_0	11.5 m/s	Chao et al.[41] Gupta et al.[40]
Human mouth opening d	2 cm	Zhu et al.[48,49]
Average cough volume measured V	1.4 l	Zhu et al.[48,49] Mahajan et al.[50] Gupta et al.[40]
Average mass of the saliva droplets per cough	6.8 mg	Zhu et al.[48,49]
Density of the jet ρ	7 kg/m³	Zhu et al.[48,49]

TABLE II. Principal parameters of test T2.

T2—sneeze		
Temperature (T)	32 °C with 20° ambient	Zhu et al.[48,49]
Average expiration air velocity during coughing U_0	22 m/s	La Rosa et al.[53]
Human mouth opening d	2 cm	Zhu et al.[48,49]
Average cough volume measured V	3 l	Zhu et al.[48,49] Mahajan et al.[50] Gupta et al.[40]
Average mass of the saliva droplets per cough	6.8 mg	Zhu et al.[48,49]
Density of the jet ρ	3 kg/m³	Zhu et al.[48,49]

a continuum of sizes within it. According to the experimental studies of Zhu et al.,[48,49] the total mass of saliva per cough varied within a range of 6–8 mg, depending on the subject, and averaged about 6.7 mg. The maximum amount of air that could be expelled in a coughing/sneezing process was smaller than the lung capacity, averaging 4 l for an adult male. Considering an average cough volume of about 1.4 l[40,48–50] and an average sneeze volume of about 3 l,[51,52] the density of jets representing coughs and sneezes is about 7 and 3 kg/m^3, respectively.[40,49]

The PIV (Particle Image Velocimetry) studies by Zhu et al.[48,49] indicated that the peak cough velocity varied from 6 to 22 m/s, with an average of 11.2 m/s, and Chao et al.[41] reported that the maximum air velocity during coughing by a male volunteer was 13.2 m/s and that by a female volunteer was 10.2 m/s; the average air velocity was 11.7 m/s. Therefore, the T1 simulations assumed that droplets were injected into the computational domain with the same instantaneous velocity as that of the pulse airflow, and a particle jet representing a single cough had a velocity U_0 of 11.5 m/s at the nozzle. The duration of the pulse air jet was 500 ms, taken from the experiments by Gupta et al.[40]

In T2, our simulations assumed that droplets were injected into the domain with the instantaneous velocity of the pulse airflow; a particle jet representing a single sneeze had a velocity U_0 of 22 m/s at the nozzle, as in the experimental data of La Rosa et al.[53] The duration of the pulse air jet was 300 ms.[54]

IV. RESULTS

The validity of the numerical scheme adopted here was checked against the observations of real human coughs and sneezes reported by Bourouiba et al.[54]
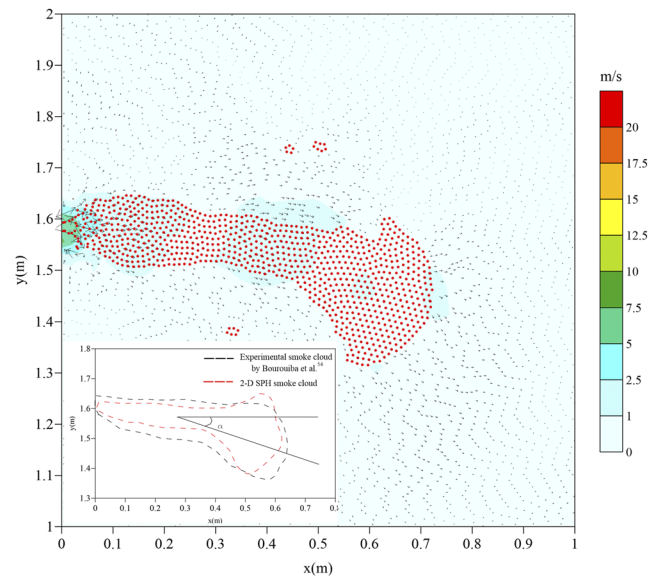

FIG. 3. Numerical air velocity fields for coughing (T1) compared with a high-speed image of a cough (inset) recorded at 1000 fps at t = 0.4 s.

Consistent with their report, Fig. 2 shows a cone-like shape of the jet cloud in the cough (test T1) at t = 0.03 s, and a maximum distance of 20 cm (horizontally away from the mouth) was found for droplets, which is of a similar order of magnitude to the experimental observations.[54] These results are in good agreement with other studies.[12,18]
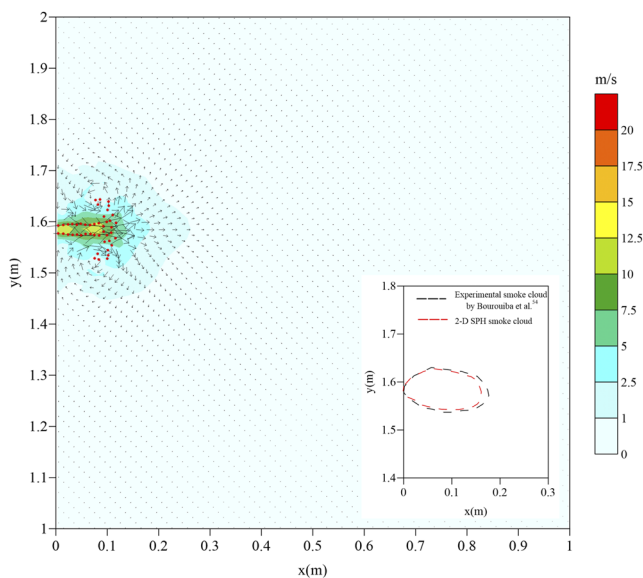

FIG. 2. Numerical air velocity fields for coughing (T1) compared with a high-speed image of a cough (inset) recorded at 1000 fps at t = 0.3 s.
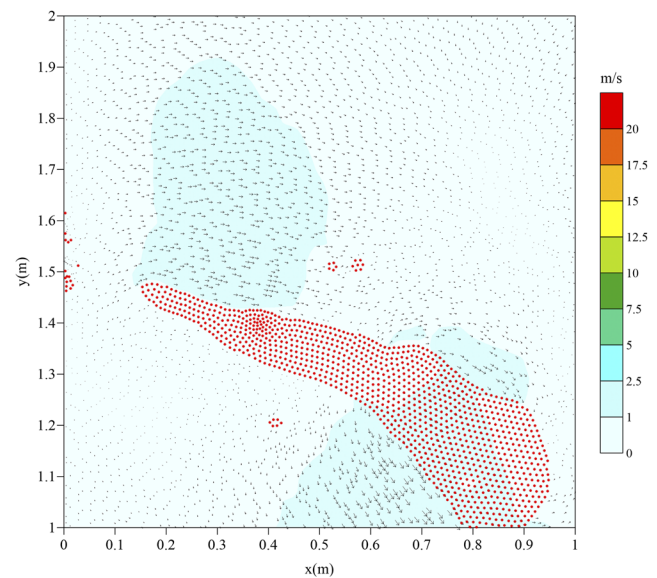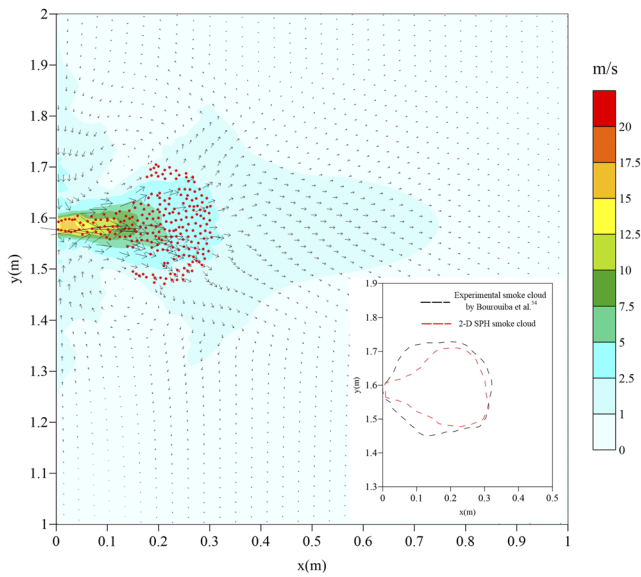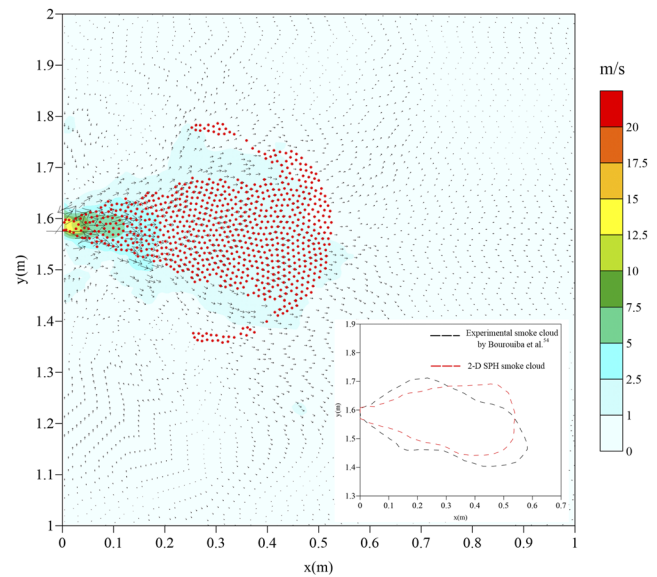

FIG. 4. Numerical air velocity fields for coughing (T1) at t = 1.0 s.

FIG. 5. Numerical air velocity fields for sneezing (T2) compared with high-speed images of a sneeze recorded at 1000 fps at t = 0.10 s.

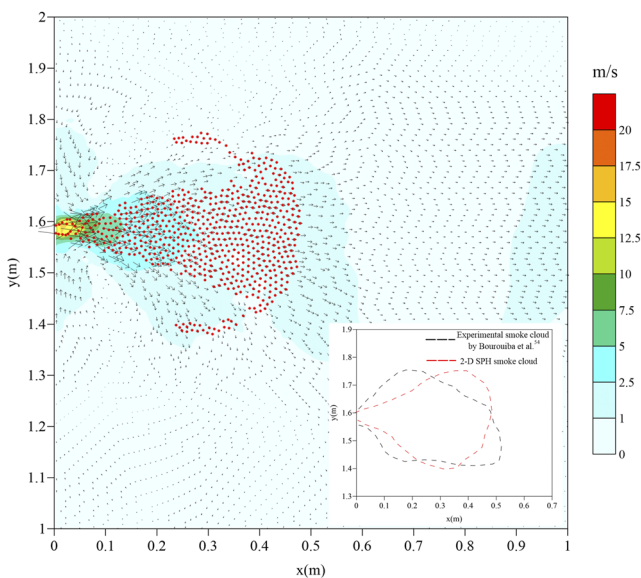

FIG. 7. Numerical air velocity fields for sneezing (T2) compared with high-speed images of a sneeze recorded at 1000 fps at t = 0.22 s.

We observed that during the applied ejection period of 0.4 s (Fig. 2), the carrier fluid flow was at the maximum velocity of 7.5 m/s, which drops down gradually after closure of the mouth.

Figure 3 shows that a smoke cloud in a cough was directed downward at an angle 24° from the horizontal. This again is in good agreement with the experiments.[54] Figure 4 shows a rapid reduction

in the velocity of the jet cloud so that at t = 1.0 s, the pulse air jet was at a horizontal distance of 100 cm and a vertical distance of 60 cm from the source. After 1 s, all droplets did not exceed a horizontal distance of 100 cm away from the mouth, confirming the numerical results by Dbouk and Drikakis.[12] The mean horizontal jet velocity decreased from 7.2 m/s at t = 0.03 s to 1.65 m/s at 0.3 s, 1.14 m/s at 0.4 s, and 0.78 m/s at 1 s.

FIG. 6. Numerical air velocity fields for sneezing (T2) compared with high-speed images of a sneeze recorded at 1000 fps at t = 0.16 s.
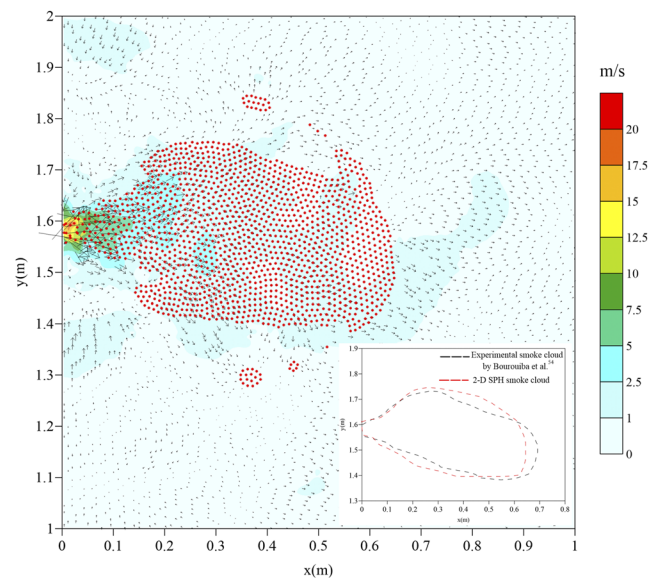
FIG. 8. Numerical air velocity fields for sneezing (T2) compared with high-speed images of a sneeze recorded at 1000 fps at t = 0.34 s.

Figures 5–8 show the simulated temporal evolution of a sneeze between 0 and 0.34 s, and this is compared to the trajectories of droplets emitted during a real human sneeze.[54] The results show that the behavior of the simulated jet is consistent with the experiments of Bourouiba et al.[54] The first image (Fig. 5) shows a cone-like shape of the jet cloud and a high density of droplets emitted by the sneeze. These results are consistent with those of Bourouiba et al.[54] in that the sneeze creates a strong pulse air jet at a distance of 70 cm from the source at t = 0.34 s and the smoke cloud that was initially directed horizontally veers downward (Fig. 8). Using the maximum numerical ejection speed and geometry at t = 0.34 s,

we estimate a typical Reynolds number of 4×10^4, as observed experimentally by Bourouiba et al.[54] The mean horizontal jet velocity decreased from 5 m/s at t = 0.10 s to 2.4 m/s at 0.16 s, 1.9 m/s at 0.2 s, 1.6 m/s at 0.34 s, 0.74 m/s at 1 s, 0.4 m/s at 2 s, and 0.1 m/s at 3 s.

Figures 9(a)–9(d) shows a rapid reduction in the smoke cloud's horizontal velocity so that after t = 1 s, no significant horizontal displacement could be observed, while a significant downward vertical displacement was observed. Figure 9(d) shows that at t = 1.0 s, the distance of the pulse air jet from the source was 100 cm horizontally and 40 cm vertically.
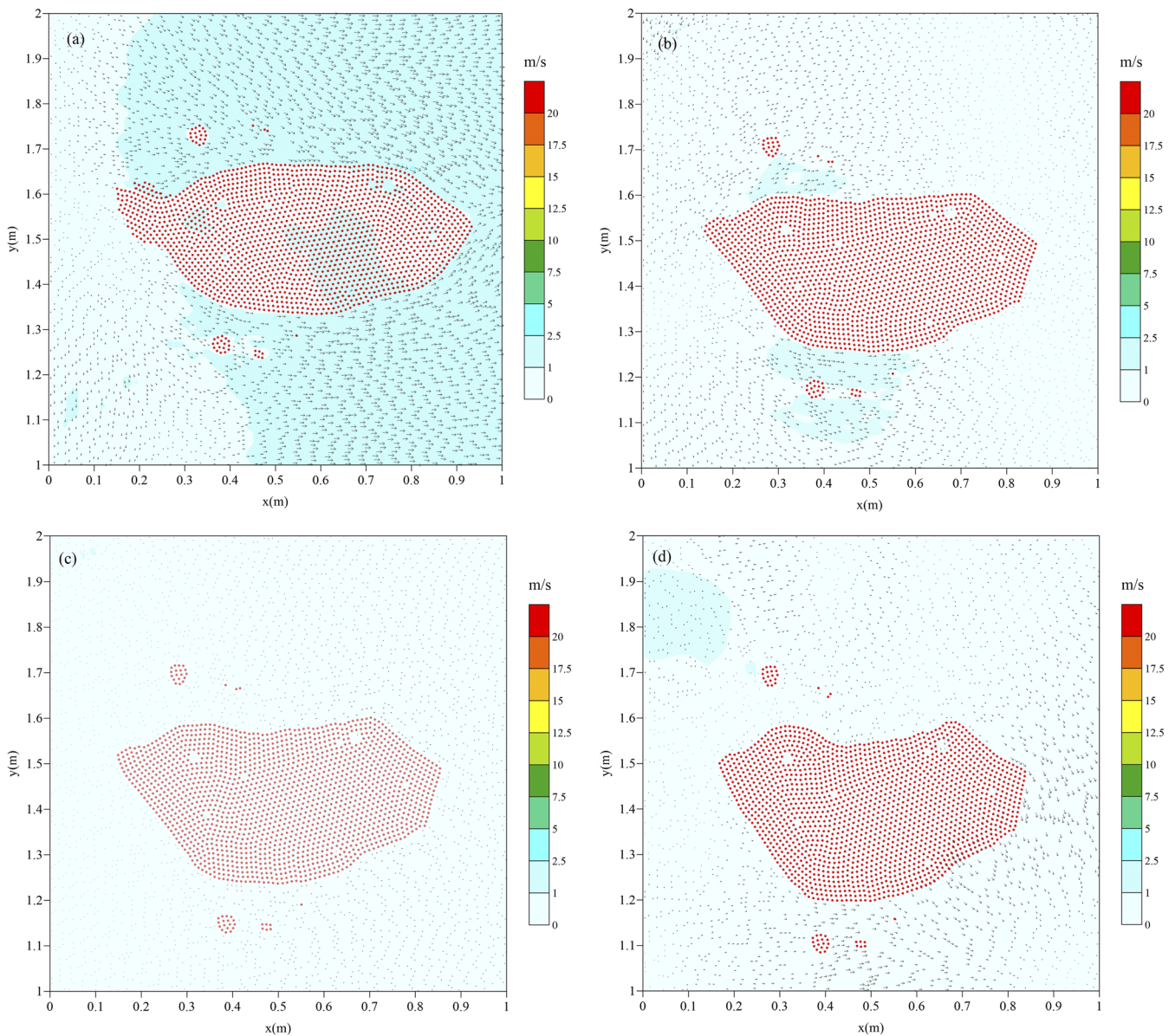

FIG. 9. Numerical air velocity fields for sneezing (T2) at (a) 1 s, (b) 2 s, (c) 3 s, and (d) 4.5 s.
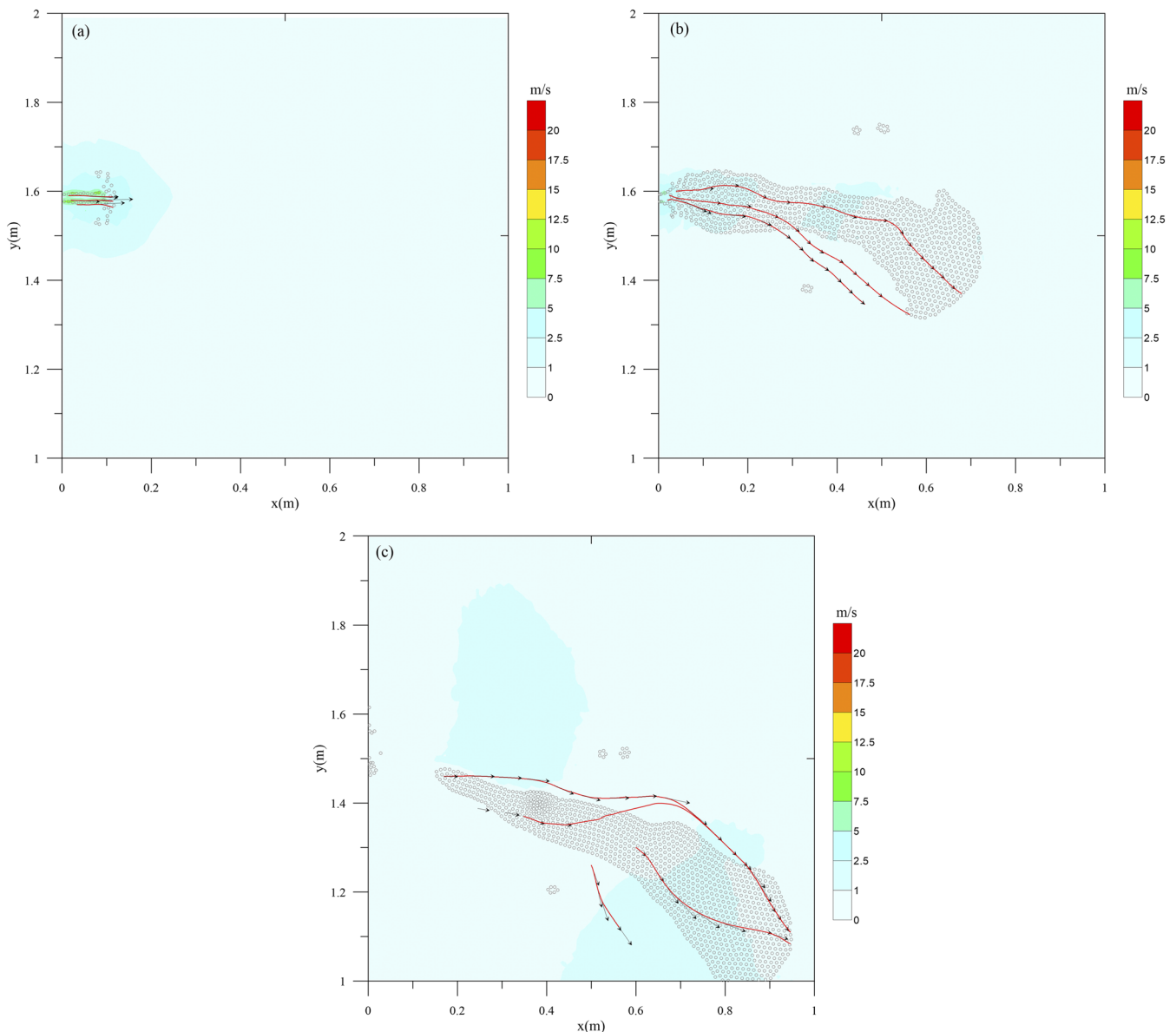
FIG. 10. Streamlines of jet cloud for coughing (T1) at (a) t = 0.02 s, (b) t = 0.4 s, and (c) t = 1 s.

A. Analysis of jet cloud behavior

The streamlines describing the trajectories of the jet cloud for coughing (T1) and sneezing (T2) reveal three phases of movement: the first phase is dominated by no-buoyancy jet-like dynamics at a high speed [Figs. 10(a) and 11(a)], the second phase is dominated by negative buoyancy [Figs. 10(b) and 11(b)], and the third phase is dominated by gravity that deflects the cloud downward [Figs. 10(c) and 11(c)]. However, the third phase of sneezing (T2) occurs later because the jet cloud is dominated by buoyancy during the period t = 1–3 s following a reduction in the horizontal velocity. Therefore, for test T2, the second phase is less evident because of smaller differences in density between the air and jet particles.

V. DISCUSSION

For test T2 at time t = 0.34 s, it can be seen from Fig. 12 that two different modes of jet behavior (shown as triangles vs circles) are largely a function of distance from the human mouth. These results highlight that in mode 1 (triangles in Fig. 12), dilution C_0/C increases very rapidly with the distance from the nozzle, and the maximum dilution occurs at a distance $x/d = 10$ from the human mouth. In mode 2 (circles in Fig. 12), however, dilution C_0/C is only weakly influenced by the distance from the human mouth, and a local average dilution of 1.95 is observed. Generally, the data follow an exponential law for $x/d \lesssim 10$, which is still in the region where the jet is developing and
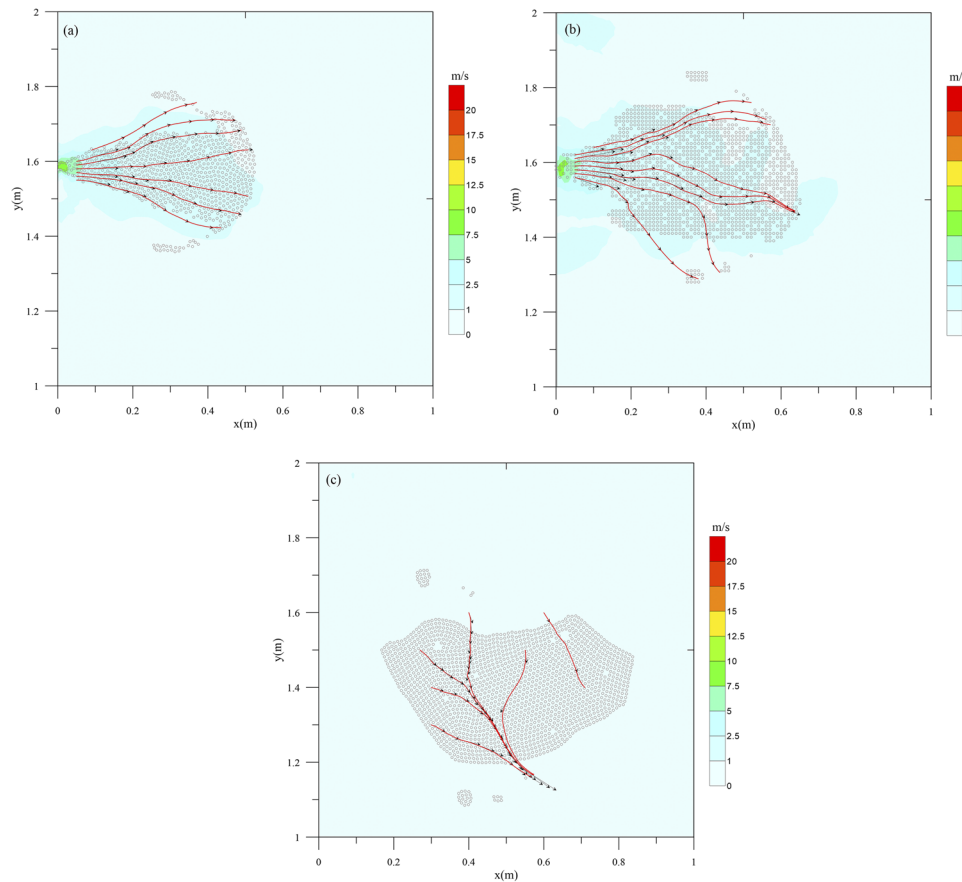
FIG. 11. Streamlines of jet cloud for sneezing (T2) at (a) t = 0.22 s, (b) t = 0.34 s, and (c) t = 4.5 s.
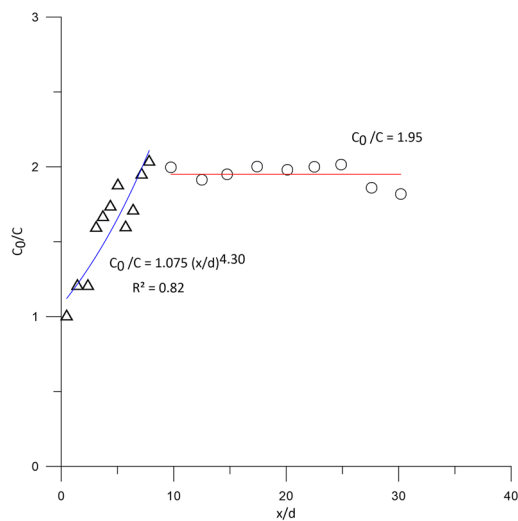

FIG. 12. Curve dilution for sneezing. The triangles and circles indicate two modes of the dependence of the concentration ratio, C_0/C, on the downstream distance, x/d. C_0 = concentration of the jet (human mouth effluent) at the nozzle, C = local concentration, and d = diameter of the human mouth opening.

approaches an asymptote for $x/d \gtrsim 10$, where a cloud-like shape is observed.

VI. CONCLUSION

The objective of the present work was to investigate the fluid dynamics of cough/sneeze events to understand the transmission dynamics of respiratory infections. 2D SPH simulations have utilized a validated Weakly Compressible SPH (WCSPH) scheme to examine the transport characteristics of droplets produced by coughing and sneezing. The SPH model was validated by comparing the simulated results with the experiments on real human coughs and sneezes by Bourouiba et al.,[54] showing that the simulations were consistent with experimental data.

The streamlines of a jet cloud for coughing (T1) and sneezing (T2) show that it evolves in three phases: the first phase is dominated by no-buoyancy jet-like dynamics characterized by high-speed, the second phase is dominated by negative buoyancy, and the third phase is dominated by gravity that deflects the cloud downward.

The high viral load in droplets of asymptomatic hosts that are expelled during respiratory activities is contributing to the rapid growth of the COVID-19 global pandemic.[55] Therefore, to study transmission dynamics of respiratory infections, simulations of the

dilution curve have been carried out for a sneeze event, which is a major source of pathogen-carrying droplets in indoor air. Two different modes of jet behavior differentiated by the distance from the human mouth were identified. In mode 1, dilution C_0/C increases very rapidly with the distance from the mouth (nozzle in the simulations), and maximum dilution occurs at a distance x/d = 10. In mode 2, dilution C_0/C is instead weakly influenced by the distance from the mouth, and a local average dilution of 1.95 is observed. Generally, C_0/C behaves exponentially for $x/d \lesssim 10$ where the jet is still developing and approaches an asymptote for $x/d \gtrsim 10$ where a cloud-like shape is observed.

Therefore, the results of these simulations can help determine the separation distance from an infected person that minimizes respiratory transmission. This work is helpful to the studies on the spread of COVID-19 and to any such pandemic in the future.

ACKNOWLEDGMENTS

DATA AVAILABILITY

The data that support the findings of this study are available from the corresponding author upon reasonable request.

REFERENCES

[1] W. E. Bischoff, K. Swett, I. Leng, and T. R. Peters, "Exposure to influenza virus aerosols during routine patient care," J. Infect. Dis. **207**(7), 1037–1046 (2013).

[2] W. G. Lindsley, T. A. Pearce, J. B. Hudnall, K. A. Davis, S. M. Davis, M. A. Fisher, R. Khakoo, J. E. Palmer, K. E. Clark, I. Celik, C. C. Coffey, F. M. Blachere, and D. H. Beezhold, "Quantity and size distribution of cough-generated aerosol particles produced by influenza patients during and after illness," J. Occup. Environ. Hyg. **9**(7), 443–449 (2012).

[3] W. G. Lindsley, J. D. Noti, F. M. Blachere, R. E. Thewlis, S. B. Martin, S. Othumpangat, B. Noorbakhsh, W. T. Goldsmith, A. Vishnu, J. E. Palmer, K. E. Clark, and D. H. Beezhold, "Viable influenza A virus in airborne particles from human coughs," J. Occup. Environ. Hyg. **12**(2), 107–113 (2015).

[4] M.-R. Pendar and J. C. Páscoa, "Numerical modeling of the distribution of virus carrying saliva droplets during sneeze and cough," Phys. Fluids **32**, 083305 (2020).

[5] S. Verma, M. Dhanak, and J. Frankenfield, "Visualizing the effectiveness of face masks in obstructing respiratory jets," Phys. Fluids **32**(6), 061708 (2020).

[6] R. Bhardwaj and A. Agrawal, "Likelihood of survival of coronavirus in a respiratory droplet deposited on a solid surface," Phys. Fluids **32**(6), 061704 (2020).

[7] R. Mittal, R. Ni, and J.-H. Seo, "The flow physics of COVID-19," J. Fluid Mech. **894**, F2 (2020).

[8] L. Bourouiba, "Turbulent gas clouds and respiratory pathogen emissions potential implications for reducing transmission of COVID-19," JAMA, J. Am. Med. Assoc. **323**(18), 1837–1838 (2020).

[9] S. Asadi, N. Bouvier, A. S. Wexler, and W. D. Ristenpart, "The coronavirus pandemic and aerosols: Does COVID-19 transmit via expiratory particles?," Aerosol Sci. Technol. **54**(6), 635–638 (2020).

[10] F. Petrini, S. Manenti, K. Gkoumas, and F. Bontempi, "Structural design and analysis of offshore wind turbines from a system point of view," Wind Eng. **34**, 85–108 (2010).

[11] P. D. Stein and H. N. Sabbah, "Turbulent blood flow in the ascending aorta of humans with normal and diseased aortic valves," Circ. Res. **39**(1), 58–65 (1976).

[12] T. Dbouk and D. Drikakis, "On coughing and airborne droplet transmission to humans," Phys. Fluids **32**, 053310 (2020).

[13] B. Wang, H. Wu, and X.-F. Wan, "Transport and fate of human expiratory droplets—A modeling approach," Phys. Fluids **32**, 083307 (2020).

[14] B. Bostanci Ceran, A. Karakoç, and E. Taciroğlu, "Airborne pathogen projection during ophthalmic examination," Graefe's Arch. Clin. Exp. Ophthalmol. **258**, 2275–2282 (2020).

[15] P. J. Mucha, S.-Y. Tee, D. A. Weitz, B. I. Shraiman, and M. P. Brenner, "A model for velocity fluctuations in sedimentation," J. Fluid Mech. **501**, 71–104 (2004).

[16] A.-K. Tornberg and M. J. Shelley, "Simulating the dynamics and interactions of flexible fibers in Stokes flow," J. Comput. Phys. **196**, 8–40 (2004).

[17] J. Wang and A. Layton, "Numerical simulations of fiber sedimentation in Navier–Stokes flows," Commun. Comput. Phys. **5**(1), 61–83 (2009).

[18] T. Dbouk and D. Drikakis, "On respiratory droplets and face masks," Phys. Fluids **32**(6), 063303 (2020).

[19] D. De Padova and M. Mossa, "Modelling fluid–structure interactions: A survey of methods and experimental verification," Proc. Inst. Civ. Eng. **173**, 159 (2020).

[20] D. De Padova, R. A. Dalrymple, and M. Mossa, "Analysis of the artificial viscosity in the smoothed particle hydrodynamics modelling of regular waves," J. Hydraul. Res. **52**, 836–848 (2014).

[21] D. De Padova, M. Brocchini, F. Buriani, S. Corvaro, F. De Serio, M. Mossa, and S. Sibilla, "Experimental and numerical investigation of prebreaking and breaking vorticity within a plunging breaker," Water **10**(4), 387 (2018).

[22] D. De Padova, M. Ben Meftah, F. De Serio, M. Mossa, and S. Sibilla, "Characteristics of breaking vorticity in spilling and plunging waves," Environ. Fluid Mech. **20**(2), 233–260 (2020).

[23] C. V. Makris, C. D. Memos, and Y. N. Krestenitis, "Numerical modeling of surf zone dynamics under weakly plunging breakers with SPH method," Ocean Modell. **98**, 12–35 (2016).

[24] D. De Padova, M. Mossa, S. Sibilla, and E. Torti, "3D SPH modelling of hydraulic jump in a very large channel," J. Hydraul. Res. **51**(2), 158–173 (2013).

[25] D. De Padova, M. Mossa, and S. Sibilla, "SPH modelling of hydraulic jump oscillations at an abrupt drop," Water **9**(10), 790 (2017).

[26] D. De Padova, M. Mossa, and S. Sibilla, "SPH numerical investigation of characteristics of hydraulic jumps," Environ. Fluid Mech. **18**(4), 849–870 (2018).

[27] D. De Padova, M. Mossa, and S. Sibilla, "SPH numerical investigation of the characteristics of an oscillating hydraulic jump at an abrupt drop," J. Hydrodyn. **30**, 106 (2018).

[28] E. Bertevas, T. Tran-Duc, K. Le-Cao, B. C. Khoo, and N. Phan-Thien, "A smoothed particle hydrodynamics (SPH) formulation of a two-phase mixture model and its application to turbulent sediment transport," Phys. Fluids **31**, 103303 (2019).

[29] H. Yang, R. Li, P. Lin, et al. "Two-phase smooth particle hydrodynamics modeling of air-water interface in aerated flows," Sci. China Technol. Sci. **60**, 479–490 (2017).

[30] M. Landrini, A. Colagrossi, M. Greco, and M. P. Tulin, "Gridless simulations of splashing processes and near-shore bore propagation," J. Fluid Mech. **591**, 183–213 (2007).

[31] D. De Padova, M. Mossa, and S. Sibilla, "SPH numerical investigation of the velocity field and vorticity generation within a hydrofoil induced spilling breaker," Environ. Fluid Mech. **16**(1), 267–287 (2016).

[32] X. Y. Cao, L. Tao, A.-M. Zhang, and F. R. Ming, "Smoothed particle hydrodynamics (SPH) model for coupled analysis of a damaged ship with internal sloshing in beam seas," Phys. Fluids **31**, 032103 (2019).

[33] D. De Padova, M. Mossa, and S. Sibilla, "Characteristics of non buoyant jets in a wave environment investigated numerically by SPH," Environ. Fluid Mech. **20**(1), 189–202 (2020).

[34] D. De Padova, M. Mossa, and S. Sibilla, "Numerical investigation of the behaviour of jets in a wave environment," J. Hydraul. Res. **58**, 618 (2019).

[35] S. Barile, D. De Padova, M. Mossa, and S. Sibilla, "Theoretical analysis and numerical simulations of turbulent jets in a wave environment," Phys. Fluids **32**, 035105 (2020).

[36] A. Colagrossi and M. Landrini, "Numerical simulation of interfacial flows by smoothed particle hydrodynamics," J. Comput. Phys. **191**(2), 448–475 (2003).

[37] B. E. Launder and D. B. Spalding, "The numerical computation of turbulent flows," Comput. Methods Appl. Mech. Eng. **3**, 269–289 (1974).

[38] D. Violeau and R. Issa, "Numerical modelling of complex turbulent free-surface flows with the SPH method: An overview," Int. J. Numer. Methods Fluids **53**, 277–304 (2007).

[39] M. Gomez-Gesteira, B. D. Rogers, R. A. Dalrymple, and A. J. C. Crespo, "State-of-the-art of classical SPH for free-surface flows," J. Hydraul. Res. **48**, 6–27 (2010).

[40] J. K. Gupta, C.-H. Lin, and Q. Chen, "Flow dynamics and characterization of a cough," Indoor Air **19**, 517–525 (2009).

[41] C. Y. H. Chao, M. P. Wan, L. Morawska, G. R. Johnson, Z. D. Ristovski, M. Hargreaves, K. Mengersen, S. Corbett, Y. Li, X. Xie, and D. Katoshevski, "Characterization of expiration air jets and droplet size distributions immediately at the mouth opening," J. Aerosol Sci. **40**(2), 122–133 (2009).

[42] C. I. Fairchild and J. F. Stampfer, "Particle concentration in exhaled breath," Am. Ind. Hyg. Assoc. J. **48**, 948–949 (1987).

[43] K. P. Fennelly, J. W. Martyny, K. E. Fulton, I. M. Orme, D. M. Cave, and L. B. Heifets, "Cough-generated aerosols of *Mycobacterium tuberculosis*: A new method to study infectiousness," Am. J. Respir. Crit. Care Med. **169**, 604–609 (2004).

[44] L. Morawska, "Droplet fate in indoor environments, or can we prevent the spread of infection?," Indoor Air **16**, 335–347 (2006).

[45] R. S. Papineni and F. S. Rosenthal, "The size distribution of droplets in the exhaled breath of healthy human subjects," J. Aerosol Med. **10**, 105–116 (1997).

[46] X. Xie, Y. Li, H. Sun, and L. Liu, "Exhaled droplets due to talking and coughing," J. R. Soc., Interface **6**, S703–S714 (2009).

[47] S. Yang, G. W. M. Lee, C.-M. Chen, C.-C. Wu, and K.-P. Yu, "The size and concentration of droplets generated by coughing in human subjects," J. Aerosol Med. **20**, 484–494 (2007).

[48] S. Zhu, S. Kato, and J. H. Yang, "Investigation into airborne transport characteristics of air-flow due to coughing in a stagnant room environment," ASHRAE Trans. **112**, 123–133 (2006).

[49] S. Zhu, S. Kato, and J.-H. Yang, "Study on transport characteristics of saliva droplets produced by coughing in a calm indoor environment," Build. Environ. **41**, 1691–1702 (2006b).

[50] R. P. Mahajan, P. Singh, G. E. Murty, and A. R. Aitkenhead, "Relationship between expired lung volume, peak flow rate and peak velocity time during a cough manoeuvre," Br. J. Anaesth. **72**, 298–301 (1994).

[51] B. Zhao, Z. Zhang, and X. Li, "Numerical study of transport of droplets or particles generated by respiratory system indoors," Build. Environ. **40**, 1032–1039 (2005).

[52] X. Li, Y. Shang, Y. Yan, L. Yang, and J. Tu, "Modelling of evaporation of cough droplets in inhomogeneous humidity fields using the multi-component Eulerian-Lagrangian approach," Build. Environ. **128**, 68–76 (2018).

[53] G. La Rosa, M. Fratini, S. Della Libera, M. Iaconelli, and M. Muscillo, "Viral infections acquired indoors through airborne, droplet or contact transmission," Ann. Ist. Super. Sanita **49**(2), 124–132 (2013).

[54] L. Bourouiba, E. Dehandschoewercker, and J. W. M. Bush, "Violent expiratory events: On coughing and sneezing," J. Fluid Mech. **745**, 537–563 (2014).

[55] Y. Bai, L. Yao, T. Wei, F. Tian, D.-Y. Jin, L. Chen, and M. Wang, "Presumed asymptomatic carrier transmission of COVID-19," JAMA, J. Am. Med. Assoc. **323**(14), 1406–1407 (2020).